ELSEVIER

Contents lists available at ScienceDirect

### Journal of Manufacturing Processes

journal homepage: www.elsevier.com/locate/manpro





## In-situ monitoring and ex-situ elasticity mapping of laser induced metal melting pool using ultrasound: Numerical and experimental approaches

Teng Yang <sup>a,b,d</sup>, Yuqi Jin <sup>a,c</sup>, Brian Squires <sup>a</sup>, Tae-Youl Choi <sup>c</sup>, Narendra B. Dahotre <sup>b,d</sup>, Arup Neogi <sup>a,d,\*</sup>

- <sup>a</sup> Department of Physics, University of North Texas, Denton, TX 76203, USA
- <sup>b</sup> Department of Materials Science and Engineering, University of North Texas, Denton, TX 76207, USA
- <sup>c</sup> Department of Mechanical Engineering, University of North Texas, Denton, TX 76207, USA
- <sup>d</sup> Center for Agile and Adaptive Additive Manufacturing, University of North Texas, Denton, TX 76207, USA

#### ARTICLE INFO

# Keywords: In-situ monitoring Ultrasonic elastography Ex-situ inspection Laser aided manufacturing Laser melting process Melting pool Ultrasound monitoring Elasticity

#### ABSTRACT

This study presents novel in-situ monitoring of the melting pool behavior and ex-situ inspection of the heat-affected softening in gallium metal using an ultrasonic technique. In the laser welding and laser melting additive manufacturing process, understanding the melting pool's behavior is necessary but challenging. Optical, thermal, and radiational imaging methods provide valuable information but are limited due to the lack of depth and material properties information. An ultrasonic time of flight measurement monitoring technique is numerically and experimentally used to study the behavior of laser-induced melting pools, including phase transition, pool initialization and growth, and solidification in real-time. Besides, a dynamic bulk modulus elastography scan was demonstrated to visualize the laser-heating induced mechanical property reduction as an ex-situ inspection process which can be an in-situ process in the future. The laser softened area had a drop in the elasticity resembling a melt pool's shape. With the continuous development, the unique technique would be suitable and helpful to be used as a diagnostic tool to monitor laser welding, laser melting-based additive manufacturing, and other melt-solidify processing systems.

#### 1. Introduction

Understanding metals and alloys' melting and solidification is important for enhancing manufacturing processes such as welding [1] and metal 3D printing [2]. The physical properties of the processed workpieces are highly dependent on the manufacturing methodology [3,4], especially cooling rate related microstructure formation [5] induced various dynamic elasticities [6] and plasticities [7]. The parts experience a re-melting and natural solidification process and result in enlarged grain size, which reduces the mechanical performance [4] and corrosion resistance [8]. This phenomenon is commonly observed in laser welding [9] and laser melting additive manufacturing [9,10]. The melting and solidification occur in localized small melting pools [1,2] within the bulk scale specimens. It can be spatially inhomogeneous for structures with complex shapes, which introduces more challenges to numerically predict or experimentally characterize the properties of the manufactured materials. Furthermore, the sample fabrication status depends on the processing parameters such as laser power [11], scan speed [12], and laser beam scanning paths [13]. An accurate melting pool monitoring method corroborated with a close-loop feedback-controlling system would be useful to prevent unexpected defects [14] or flaws [15] before initialization in the future.

The observation of the melting pool behavior in metal/alloy material systems was demonstrated by various approaches, including spectral [16,17], optical [18], thermal [19], and radiational [20] techniques. Laser-induced breakdown spectroscopy (LIBS) collects optical or even plasmonic emission of a sample induced by a high-power laser [21]. With just an additional spectrometer needed in setup, this technique is broadly used in metal/alloy AM as a melting pool monitoring method to collect chemical composition information from the pool [22]. However, the spectrums were noisy and complicated when the technique was monitored the welding or printing processing of high entropy alloys or superalloys with numerous compositions [22]. Optical [23] or thermal camera [24] imaging was another method for the melt pool monitoring approach by visualizing melt pools' shape and temperature distribution from the top view. However, those techniques were lacked on depth

https://doi.org/10.1016/j.jmapro.2021.08.031

Received 6 June 2021; Received in revised form 20 August 2021; Accepted 23 August 2021 Available online 24 September 2021

<sup>\*</sup> Corresponding author at: Department of Physics, University of North Texas, Denton, TX 76203, USA. *E-mail address:* arupn@yahoo.com (A. Neogi).

information which was also an important part of melting pool behaviors. Another recent work demonstrated X-ray imaging of melting pool cross-section in the in-situ setup on a thin printing sample [25] which showed high imaging clarity on the experimental obtained melting pool. However, the resolution or the imaging capability might be impacted when the sample's volume increased. All the listed methods are necessary and provide unique information about the melting pool behaviors during laser aided manufacturing. Ultrasound technique is useful as another adding-on component to provide real-time information about the melting pool location, depth, and elasticity contrast to a solid region with pre-characterized acoustic properties of the target materials.

A high-frequency acoustic wave beyond 20 kHz has been used as a length scaler [26,27], flaw detector [28,29], and elasticity mapper [30–32]. Measuring object length (d) by an acoustic wave is usually performed by the time of flight [33] methods with known speed of sound values of the target media as d = 0.5 c t, where c and t are speed of sound value and the time for pulse traveling of round-trip. Ultrasound discontinuity detection is the most common application of highfrequency acoustic waves in manufacturing [34] and biomedical [35] applications. The technique is based on the acoustic impedance mismatch-induced reflection. Based on the temporal position and amplitude, the discontinuity can be located spatially [28]. In the welding field, ultrasound detection on the products was developed to evaluate the quality of the welded joints by measured the discontinuity [36-39]. The technique can be realized by phased array transducers for an instant defect-map with the spatial information in 2-dimensions [40,41]. For a sample with a known size and geometry, its dynamic bulk modulus (K) can be determined by measuring the acoustic impedance (Z) and speed of sound (c) as a distribution map K = Zc.

During the monitoring of melting pool, all the listed methods can provide valuable information about the behavior of melting pool during melting and solidification processes. The impedance mismatch between the solid and liquid phases regions results in reflection and imply about the relative position of interfaces within the entire sample along the wave propagation direction. The melting pool height can be estimated for a sample with a pre-characterized speed of sound values of the metal's solid and liquid phases. The amplitude of an internal echo can also provide information about the relative dynamic elasticity of the metallic structure that is being manufactured.

In this study, we realized a simplified model of laser melting solid gallium samples to show the in-situ monitoring of melting pool and exsitu inspection of laser modified areas. As the initial step of study, gallium is suitable to be a simplified model testing the feasibility of ultrasound melting pool monitoring due to its relatively slow phase transition and low melting point. Unlike most of other metals, gallium has decreasing speed of sound value but increasing density value when it transited from solid phase to liquid phase. The resulting acoustic impedance of Gallium does not have a clear drop during the phase change which other metals or alloys do and provide more energy reflected back at the solid/liquid interface. Due to its special temperature dependent impedance, gallium was considered as a challenge medium to study the monitoring of melting pool.

Before the actual monitoring, we characterized the temperature-dependent speed of sound in gallium for further estimation of the position and size of the melting pool. For properly applying the time-of-flight method for estimating location or distance, the speed of sound information of the target material was necessary. Using the characterized material properties, the feasibility of localizing the melting pool by ultrasound was then proved by numerical simulation. In experiments, we selected 1.87 watts 800 nm Femtosecond laser instead of a high power continuous laser to slow down the melting process and speed up the solidification of the gallium samples. We have performed 2 runs of ultrasonic melting pool monitoring examinations with faster and slower speeds of melting demonstrated different melting pool initiation and growth behaviors. The speed steps of the melting process were manipulated by varying the size of laser focal point and the thickness of solid

gallium sample. The experimental results showed the exceptional feasibility of ultrasound melting pool monitoring. In addition, for demonstrating the ex-situ ultrasound inspection capability of laser modified area, we performed the dynamic bulk modulus elastography scan on one of the gallium samples after it solidified back from the laser induced melting. The examined dynamic bulk modulus distribution map showed a pool-like soften region on the gallium sample due to the laserinduced melting process. This study provides a proof-of-concept demonstration of in-situ monitoring of the laser-induced melting of solid gallium samples and ex-situ inspection of the modified areas due to the femtosecond laser-metal interaction. The dynamic bulk modulus elastography scan of the irradiated laser area of the sample after it solidified following the laser-induced melting process has been used for the ex-situ diagnostics. The examined dynamic bulk modulus distribution map showed a pool-like soften region on the gallium sample due to the laser-induced melting process.

#### 2. Materials and methods

Gallium is an ideal metal for testing the feasibility of ultrasound melting pool monitoring due to its relatively slow phase transition and low melting point. The temperature-dependent acoustic properties of gallium metal were experimentally investigated before studying the laser-induced phase transition of the melting pool. Relatively low power of the radiation from an 800 nm laser source, with 100 fs pulse width and 80 MHz pulse repetitions, was applied to slow down the gallium's melting process and speed up the irradiated metal's solidification. The ultrasonic melt pool behavior was monitored for varying rates of the melting process and metal fabrication process. The melting process's speed steps were manipulated by changing the size of the laser focal point and the thickness of the solid gallium sample. The size of the laser focal point was referred to the beam diameter at the focus. The experiment results showed the exceptional feasibility of ultrasound melting pool monitoring. The initial characteristics of the speed of sound in gallium were determined using a pre-prepared bulk 25.4 mm wide cubic solid gallium that was slowly heated by infrared radiation. Simultaneously, the acoustic pulse was continuously excited for recording the time-of-flight information for calculating the speed of sound. The schematic of the experiment setup is shown in Fig. 1.

#### 2.1. Gallium melting pool detection by numerical simulation

The feasibility of using ultrasound pulse detecting the liquid phase melting pool formation and growth was firstly estimated by numerical simulation. The involved software was finite element based COMSOL Multiphysics 5.4. In its time-domain pressure acoustic module, a 6 mm width ultrasound transducer can send a 20 MHz pulse envelope written as  $x(t) = \sin (2\pi f_0 t)e^{-f_0(t-\delta T_0)2}$ , where  $f_0 = 20$  MHz,  $T_0 = 1/f_0$  and  $\delta = 3$ were the fundamental frequency, period, and delay of the pulse signal. The solid gallium sample was placed above the transducer with width and height equal to 9 mm and 3 mm. The boundary probe is located at the interface between the transducer and solid gallium sample, which collecting the acoustic pressure after the pulse is sent. The melting pools were modeled as a semi-ellipse with height and width as a and 3a on the upper surface of the solid gallium sample. The initialization and growth of the melting pool were demonstrated as the value sweeping of the factor a from 0 to 1 mm with a 0.25 mm interval. The outer boundary was set to sound hard boundary. The time-domain for time-of-flight data was recorded at 80  $T_0$  length and  $T_0/10$  interval. The averaged mesh size was about  $0.87\mu m$ . The largest mesh element has the size at  $2.67\mu m$ . The speed of sound and density values of solid and liquid phase gallium was experimentally determined as  $3255 \, m/s$  and  $5925 \, kg/m^3$  for solid-phase, 2820 m/s and 6100  $kg/m^3$  for the liquid phase.

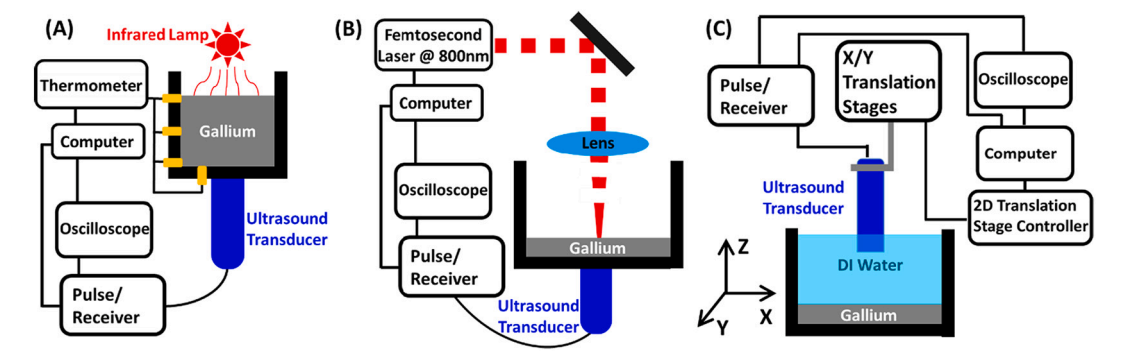


Fig. 1. Experimental setups: (A). Temperature dependent speed of sound measurement. (B). In-situ gallium melting pool monitoring experiments. (C). Dynamic bulk modulus elastography mapping.

#### 2.2. Gallium sample preparation

The solid gallium samples were prepared from melting and solidification. The gallium metal was obtained from Sigma-Aldrich 99.9% gallium in a solid-state. For molding process of the samples, the 99.9% gallium was kept in the original container, slowly heated up by convectional heat with 40  $^{\circ}$ C ambient water baths. After the solid gallium in the container was completely melted, the liquid state gallium was filled into pre-prepared testing boxes with upper side opened. The samples were naturally cooled until solidification. The testing containers for the temperature-dependent speed of the sound experiment were in a 1 in. (25.4 mm) wide cubic shape. The ultrasound monitoring experiment containers are shaped in 1.5 in. (38.1 mm) wide square in horizontal cross-section with 1.4 mm (sample 1) and 4.1 mm (sample 2) height.

## 2.3. Speed of sound and ultrasonic in-situ monitoring laser-induced melting on gallium

The experimental setup of the temperature-dependent speed of sound measurement is demonstrated in Fig. 1(A). The acoustic pulse at 20 MHz fundamental frequency was excited every 10 ms by a 0.125" diameter (3.175 mm) unfocused emersion pencil style transducer (Olympus V316-N-SU) from the bottom of the sample container. The acoustic property and thickness of the bottom wall were pre-examined by the same transducer. The electronic signal from the computercontrolled Pulse/receiver JSR Ultrasonic DPR 300. The reflected signal was collected and acquired by Tektronix MDO 3024b oscilloscope in the time domain at a 2GHz sampling rate. In the experiments, gallium samples were slowly heated up by two 600 watts infrared lamps. The temperature determined by averaging values from 4 Omega ceramic thermocouples is embedded on the container's wall as the figure illustrated. The systematic uncertainty of the time of flight measurement was dependent on the temporal interval of the acquiring equipment. In our recorded data sets, the temporal interval of the data points was 0.5  $\times$  $10^{-8}$ s which was small enough to be negligible.

The general experimental setup involved in in-situ monitoring experiments was similar to the temperature-dependent speed of sound measurement in Fig. 1(B). For the in-situ measurements, we attached a 20 MHz transducer under the plastic container filled with a solid gallium sample and used a Femtosecond laser (800 nm at 100 fs) to heat the sample. We used a thinner gallium sample and large laser power to induce a melting pool with fast speed. The power of the laser pulse was 1.87 watts. The fast transition experiment used a smaller focused laser spot of about 0.5 mm. The slow melting experiment had an enlarged focused beam-width of about 1.2 mm. The estimations of the spot size were from the pixel-counting based on the camera images.

#### 2.4. Dynamic bulk modulus and effective density elastography (EBME)

The experiment of dynamic bulk modulus and effective density elastography (EBME) were performed in a homemade 500 mm cubic acrylic water tank with infilled DI water. The gallium sample and ultrasound transducer were immersed underwater, as shown in Fig. 1(C). The scanned area of the sample was  $10 \text{ mm} \times 10 \text{ mm}$  with a 0.5 mm step interval. A square matrix was used to acquire and record the 441 position points of temporal data for each location. MATLAB® script was used to control the entire raster scanning process, including the automated movement of transducer and data acquisition. A 0.125" diameter 20 MHz unfocused emersion pencil transducer (Olympus V316-N-SU) was used for exciting a broadband pulse of 10-35 MHz (center frequency at 20 MHz) at a repetition rate of 100 Hz. The transducer was attached to a three-axis translation stage (LC Series Linear Stages of Newmark Systems, Inc.) controlled by a motion controller. A JSR Ultrasonic DPR 300 Pulser/Receiver internally operated the pulse source and time trigger, and a Tektronix MDO 3024b was used to collect the data. The data acquisition rate was the 20s for 512 signals on the same position. The 512 signals on the same position were averaged into 1 recoded waveform and displayed and collected in the oscilloscope at each measured location.

#### 3. Results

#### 3.1. Measurement of speed of sound in gallium

Before monitoring the melt pool of gallium metal due to laser irradiation, the temperature-dependent acoustic properties of solid and liquid gallium metal were experimentally measured. These measurements were performed at 20 MHz, which was the center frequency of the operating frequency band of the monitoring and inspection experiments. In Fig. 2, the sound velocity was characterized at three different heating rates. The data points were all averaged by three measurements, where the error bars indicated the standard deviation. These results depict a very consistent behavior of sound speed, which is independent of the heating rates. The sound speed was stable in the range from room temperature to 27.5  $^{\circ}\text{C}$  when the metal is in a solid-state and then from 34 °C to 37 °C when gallium is in a liquid state after phase transition. The gallium sample underwent a phase transformation from the solidstate to the liquid state as the temperature increases from 27.5 °C to 34 °C. A dramatic reduction in the velocity is observed during this stage, which was about 15% at the rate of 71.5 m/( $s^{\circ}$ C). In subfigure (B), the measured acoustic attenuation values at the solid, liquid, and during phase transition were around 0.35  $\pm$  0.01 dB/cm, 0.41  $\pm$  0.02 dB/cm, and  $0.22 \pm 0.04$  dB/cm, which were insignificant and negligible in the millimeter-scale samples monitoring experiments. Comparing with the existing literature [42,43], our experimental speed of sound values of liquid state gallium was well agreed. In the solid state, our speed of

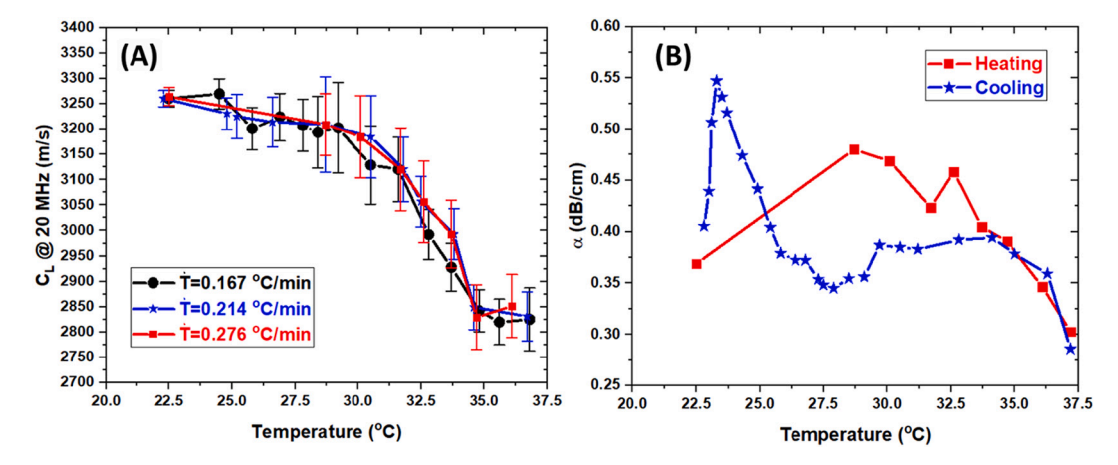


Fig. 2. (A). Temperature dependent speed of longitudinal sound wave in gallium with various heating rate. (B). Temperature dependent acoustic attenuation behavior.

sound (attenuation) values were slightly lower (higher) than the literature possibly due to the higher operating frequency comparing with the literature. The abnormal attenuation behavior of gallium was considered highly related to its abnormal density behavior between solid and liquid phases. These results were used for estimating the depth and width of the melt-pool during in-situ and ex-situ diagnostics.

## 3.2. Numerical results of ultrasound monitoring of melting pool initialization and growth

In Fig. 3, the numerical simulation results illustrated the time of flight measurements of a 3 mm thick solid gallium sample. For illustration of the measuring mechanism, we selected acoustic pressure maps obtained from time-domain numerical simulation with/without melting pool in subfigure (A) and (B). The source acoustic pulse was emitted from the bottom probe. The bottom probe kept recording the reflection signals after the source pulse was excited. At comparable time point, we

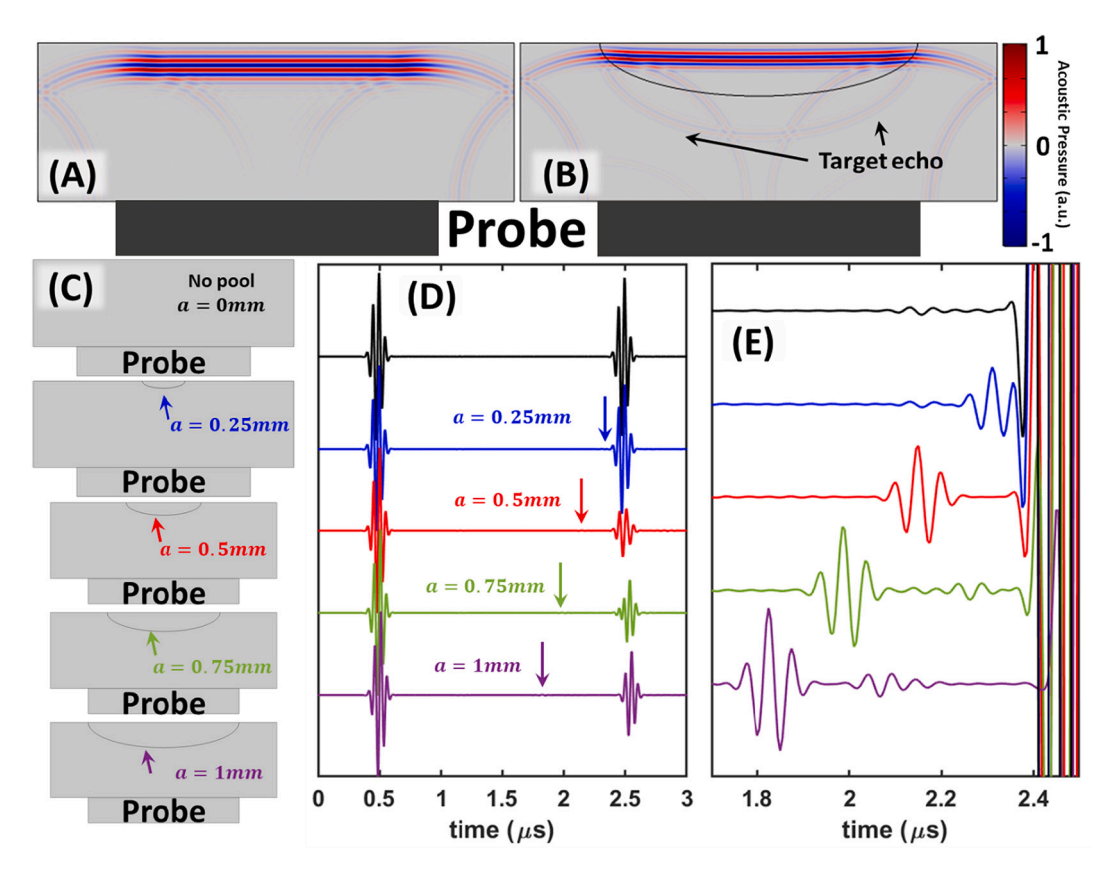


Fig. 3. (A) and (B). Visualized illustrations of the additional reflection occurred at the interface between the melting pool and solid phase material. The figures were obtained from numerical simulation. (C). The model of melting pool initialization and growth in Gallium sample from 0 mm to 1 mm with 0.25 mm steps. (D). The corresponding time of flight simulation results in the range between 0 and 3  $\mu$ s showing two major reflections from lower and upper boundaries of the solid Gallium samples. (E). The zoomed in view of the time of flight results in the range between 1.7 and 2.5  $\mu$ s showed the additional reflections due to the presence of liquid phase melting pool.

can clearly observe an additional reflection presented in (B) due to the impedance mismatch occurred at the liquid/solid interface. The additional echo was absent in the full solid gallium case (A). As subfigure (C) shows, we modeled the solid gallium without melting pool and initialized a melting pool which further grew from 0.25 mm deep to 1 mm with 0.25 mm interval. In subfigure (D), the time of flight results of all studied 5 cases were demonstrated in the range of 0  $\mu s$  to 3  $\mu s$ . The two major echoes in each case indicated the lower and upper boundaries of the solid gallium layer. The first envelope around 0.5  $\mu s$  was induced by the impedance mismatch between the transducer and the solid gallium that occurred at the interface between them. The first envelope has an identical amplitude and traveling time in all 5 cases due to the identical condition of the transducer/gallium interface. The second major envelope in all cases occurred around 2.5  $\mu s$  which was reflected from the upper surface of the gallium sample. The condition of the outer boundaries was reflecting all energy to represent the enormous impedance mismatch between gallium and ambient air in the practical experiment. The arriving time of the second major echoes had a slightly temporal delay which was proportional to the height of the melting pool which had a lower speed of sound on liquid phase gallium. Besides the two major reflected envelopes, an additional echo was able to be found in the case with the melting pool temporally arrived before the major echo from the upper surface. The additional echo had a smaller amplitude comparing with the two major echoes due to lower impedance mismatch between solid and liquid phases gallium. In subfigure (E), the presence of the additional reflections was due to of the melting pool were illustrated clearly in the zoomed-in view. Comparing with the reference time of flight data collected without melting pool on solid gallium, a 0.12 us width additional envelope appeared before the upper surface reflection in the case of 0.25 mm height melting pool. With the rise of the melting pool thickness, the additional echo arrived earlier due to the forwarded grew solid/liquid interface. The height of the melting pools was able to be estimated by the time delay between the additional echo and the upper surface echo.

#### 3.3. In-situ melting pool monitoring of rapid phase transition of gallium

The feasibility of the ultrasonic time-of-flight melting pool monitoring was demonstrated by the above numerical simulation. Experimentally, the melt pool of the selective area melting process of solid gallium irradiated by a red femtosecond laser and the subsequent solidification process is monitored using a non-invasive ultrasonic scanning process. The temporal profile of the ultrasonic pulse traveling through the gallium metal sample is shown in Fig. 4. The thickness of the gallium sample used in this experiment was known to be about 1.4 mm. The state of the gallium target due to selective laser irradiation was estimated from the distance traveled by the ultrasound pulse within the metal. It depends on the speed of sound in the medium and is modified by the gallium phase under laser irradiation. The horizontal axis was translated to axial position (in millimeters) from the experimentally recorded time-of-flight of the ultrasonic pulse. The red trace is time delayed compared to the blue trace in each of the figures. Fig. 4(A) shows the initial waveform of acoustic echoes from the gallium sample at 0 s and 60s. The trace at 0 s infers the initial condition of the pulse propagating through the sample without the laser irradiation. The red trace indicates the pulse propagation 60 s after the laser was turned on and induces metal heating. The first echo is observed from the interface between the container box and gallium metal at the 3 mm (on the x-axis) location. The second echo at 4.5 mm (x-axis) was observed from the top surface, which was the interface between gallium and ambient air. The ultrasound reflection indicated an agreed value from 2.6 mm to 4 mm. From the zoom-in figure in (A) at 60s heating time, an extra small echo appeared on the red line showing the presence of an internal discontinuity, which indicated the initialization of a melting pool inside the gallium sample. At this moment, no visible melting pool on the upper surface was observed by the camera, which means the melting pool diameter on the upper surface was smaller than the laser spot size (<1 mm). Axially, from the location of the small echo on the x-axis, the estimated that the initial melting pool height was about 29.2% depth of the gallium, which is about 0.44 mm from the upper surface. In the presence of continuous irradiation of the gallium sample for 1.5 min, a

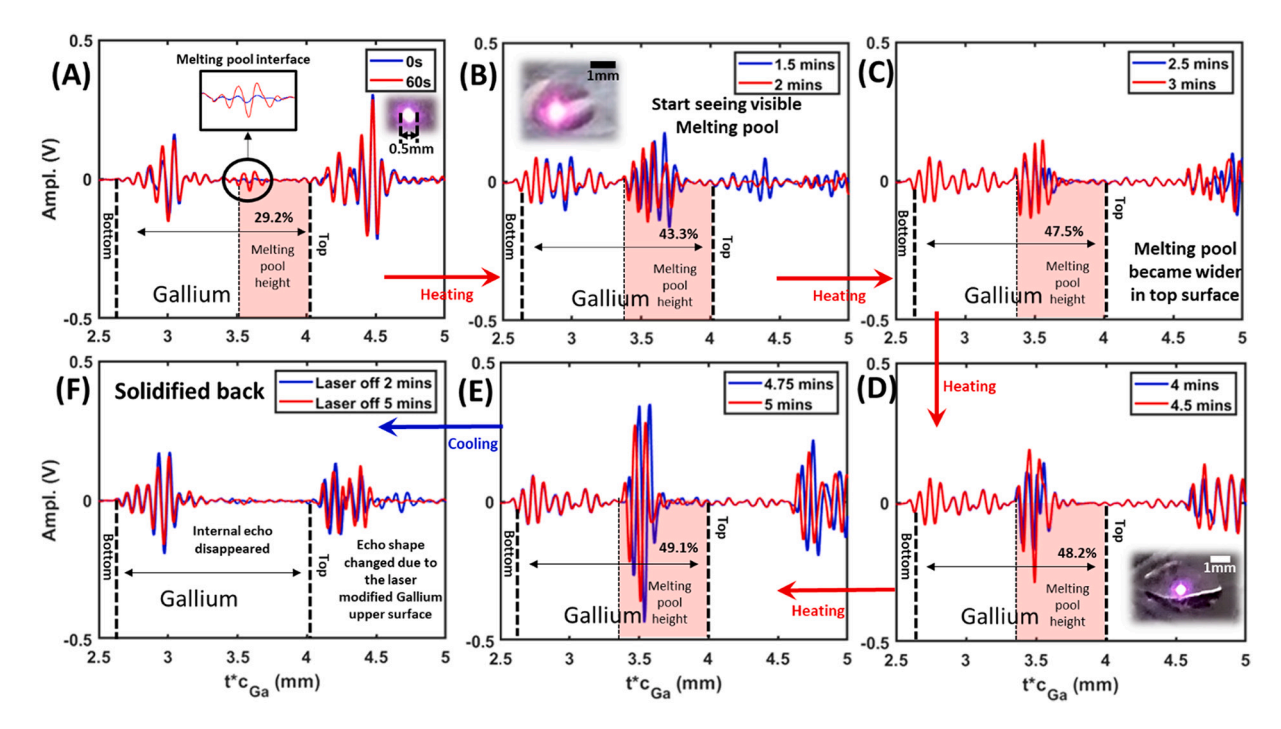


Fig. 4. In-situ melting pool monitoring of slower transition of laser-heated solid gallium sample. The thickness of the sample was about 1.4 mm. The 1.87 watts femtosecond laser was focused into a 0.5 mm focusing spot on the upper surface of gallium sample. The time of flight measurements were translated to distance of flight with the pre-tested speed of sound in gallium. (A) to (E) were the heating process. From (E) to (F), the gallium sample was cooled and solidified back after laser switching off.

visible melting pool on the upper surface appeared, as illustrated in the optical image shown in Fig. 4(B). The zoomed-in echo signal was shown within the inset of Fig. 4(A) increases at this stage, as shown in Fig. 4(B). The height of the melting pool sharply increased to 43.3% of the entire gallium sample thickness. Additionally, the amplitude of the first echo reduced due to the phase transformation of the rest of the sample thickness below the melt pool. As the laser is continuously irradiated, inducing heating within the sample, the internal echo gradually moves to the left of the time domain. It approaches the lower boundary of the gallium sample, as shown in Fig. 4(B) to (E). The amplitude of the reflected envelopes increased proportionally to the laser irradiation or heating time. As shown in Fig. 4(E), thermal equilibrium is observed when the final estimated melting pool height approaches 49.1%.

The laser was then turned off to monitor the cooling and the solidification process continuously. After 2 min of cooling, the gallium solidified back, and the internal echo is no longer observed. The discontinuity that appears due to the bottom gallium layer's phase transition and the melting pool is not observed any longer as gallium is gradually transformed back to the mixed state. The waveform also changed back to the original shape in Fig. 4(F). The shape of the second echo in Fig. 4(F) is slightly different comparing to subfigure (A) as the gallium surface at the metal-air interface was modified by the laser-induced melting process.

#### 3.4. In-situ melting pool monitoring of slow phase transition of gallium

In this experiment, the experimental setup was modified using a thicker gallium sample heated by the laser with a lower power density to obtain a slow transition behavior. In Fig. 5(A), the overall view of the recorded signals showed lower and upper boundaries of the gallium sample with a zoom-out view. The lower boundary of the gallium sample has not changed position during heating and cooling processes. However, we observed the upper boundary underwent a deformation during heating and recovering during cooling. The behavior was verified by the photograph inserted in Fig. 5 showing a deformed pool shape once the laser tuned off. The upper surface deformation was resulted by the density decreasing during the heating process. From the acoustic signals, we can estimate the maximum surface deformation occurred during the process was around 0.12 mm. Fig. 5(B) shows that the upper surface, which provided a reflection envelope, moved forward towards the bottom surface with increased laser heating time. This phenomenon indicated that the phase transformation occurred on the upper surface as a thin layer region. The density of the liquid state gallium is higher than the solid. As the laser-induced surface temperature was raised, the phase transformation within the thin layer zone underwent a volume contraction due to the abnormally increased density. The forwardmoving highlighted echo from time 0 to 4 min demonstrated the reduction of the local volume on the upper surface. Under constant laser irradiation, the initial bulk scale melting pool was observed at 18.6%

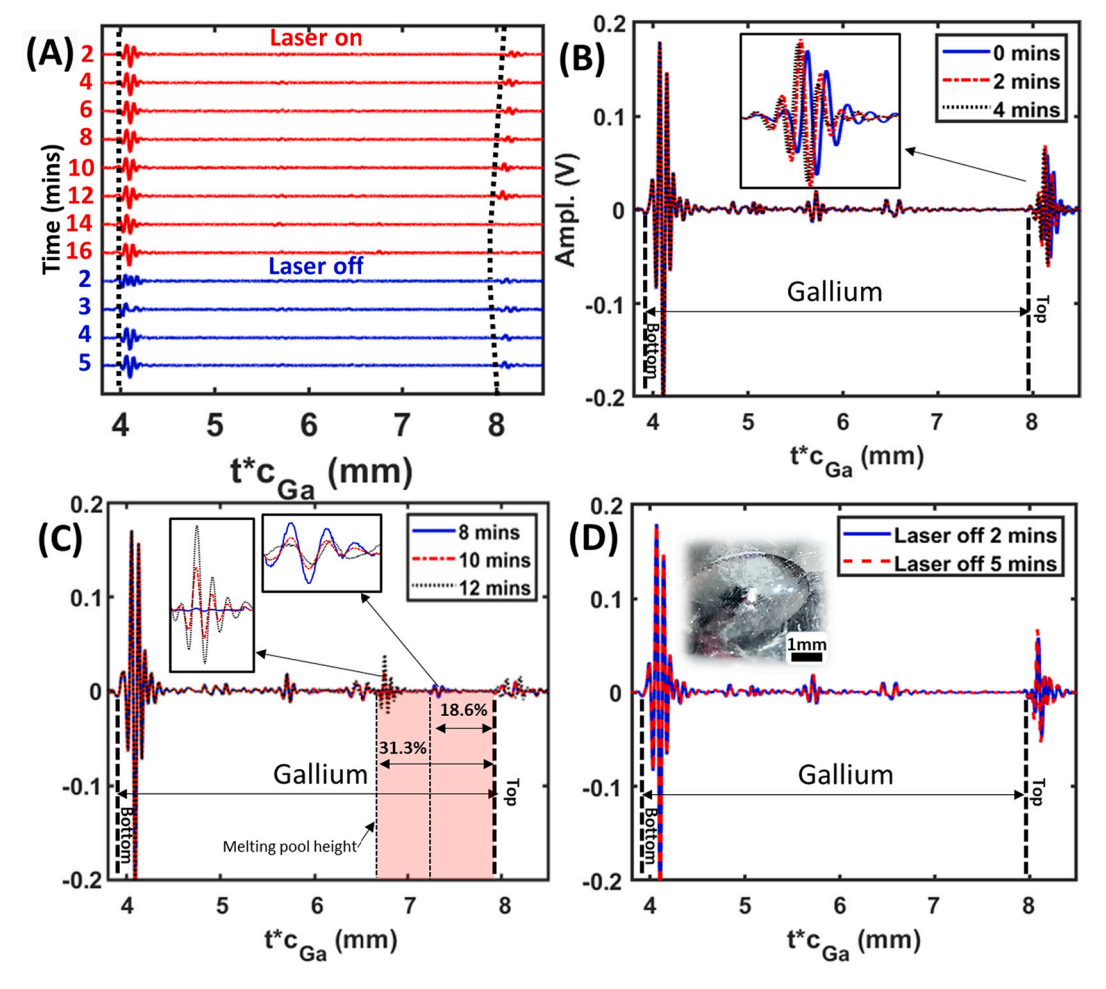


Fig. 5. In-situ melting pool monitoring of slower transition of laser-heated solid gallium sample. The thickness of the sample was about 4.1 mm. The 1.87 watts femtosecond laser was focused into a 1.2 mm focusing spot on the upper surface of gallium sample. The time of flight measurements were translated to distance of flight with the pre-tested speed of sound in gallium. (A). Overall view of the recorded reflection signals in the experiment. The red (blue) color signals referred to the heating (cooling) processes. (B) to (C) were the heating process. From (C) to (D), the gallium sample was cooled and solidified back after laser switching off. (For interpretation of the references to color in this figure legend, the reader is referred to the web version of this article.)

height away from the upper surface after 8 min heating, as shown by the blue line. The melt pool location was about 7.2 mm on the horizontal axis with a height of about 0.725 mm, as estimated from the internal echo, which was shown in the inset as a zoom-in figure of Fig. 5(C). Through the two expanded traces within the inset in subfigure (C), it can be observed that the melt pool location gets deeper at 10 min (red line). The amplitude of echo is in the intermediate position. After two more minutes, a clear melting pool signature echo was recorded at 31.3% of the original sample height showed by the black dot line. Subsequently, the recorded waveform maintained an identical shape with further heating. Fig. 5(D) illustrates the waveform of the cooling process. Within 2 min of turning off the laser to cooling the sample, the observed waveform returns to the initial state, as observed in Fig. 5(B) at t=0 min. It indicates that the gallium sample was completely solidified back to its original state.

# 3.5. Ex-situ characterization of the melt-pool of selective area laser-irradiated gallium metal

The modification of the gallium's mechanical properties under the selective laser irradiated zone was estimated from the dynamic bulk elasticity measurement developed by our group. The classical speed of sound theory was used to calculate dynamic bulk modulus: K=Zc and  $\rho=Z/c,$  where  $\rho$  is the density, c is the speed of sound, and Z is the impedance of the scanned material.

The acoustic impedance ratio between the sample and de-ionized (DI) water is:

$$\frac{Z_1}{Z_0} = \frac{-1 - \alpha - \sqrt{4\alpha + 1}}{\alpha - 2} \tag{1}$$

where the factor  $\alpha = \frac{P_1}{P_e - (Z_1 - Z_0)|P_0|}$ , and was measured from the experiment.  $P_e$  is the amplitude of the emitted pulse from the transducer.  $P_1$  and  $P_2$  are the amplitudes of the first refection and second refection, respectively.  $Z_0$  is the known acoustic impedance of ambient material (DI water).  $Z_1$  is the unknown impedance of the tested material.

Dynamic bulk modulus can be calculated using equation

$$K_{dyn} = C_L Z_0 \frac{-1 - \alpha - \sqrt{4\alpha + 1}}{\alpha - 2},$$
 (2)

where  $C_L$  is the speed of the longitudinal wave from the temporal delay between the two reflections.

Fig. 6 shows the results of ex-situ ultrasound inspection of the solid gallium sample, which has been laser melted in the previous section to estimate the dynamic bulk modulus distribution map. The total scanned area was 10 mm x10mm with 0.5 mm step intervals on both axes. Although the gallium was fully solidified back to the solid state, the heat softening effect was still observed on the sample. The capability of the elastography technique has been demonstrated by considering an anisotropic heat-transfer field along the horizontal plane. A location near the corner was selected as illustrated within the inset of Fig. 6 instead of the selective area melting of the gallium at the center of the sample. The heat diffusion to the bottom and right side of the sample was reduced by selecting this location, which led to more significant heat-affected softening around the melting pool close to those two edges. The dynamic bulk modulus elastography examined the elasticity contrast as expected. The laser softened area had a drop in the dynamic bulk modulus resembling as a melt pool's shape. The estimated modulus of the unaffected solid gallium was around 65GPa. The laser melted region had a lower modulus, which was in the range between 63GPa and 61GPa. The softened area center was located at (-0.5, -3) on the XY plane in the elastography. The dynamic elasticity drop was more critical along the Y direction at −0.5 mm on X-axis rather than along the X direction from the center. This experiment demonstrated exceptional result presented the possibility of inspecting the regions of over-heating or lack-of-heating in the metal/alloy laser-aided manufacturing products.

#### 3.6. Discussion

Our work on the ultrasound monitoring of laser-induced melting on solid gallium demonstrated the feasibility of using ultrasound to observe melting behavior in selective areas. Due to abnormal density increasing from solid to liquid phase of gallium, the acoustic impedance mismatch between solid and liquid phases gallium is not significant compared to most of other common metals or alloys, which introduced larger challenge in gallium system to distinguish the interface between solid and liquid phases regions. In the rapid phase transition process, the recorded behavior showed the initial melting process, leading to a melt pool's

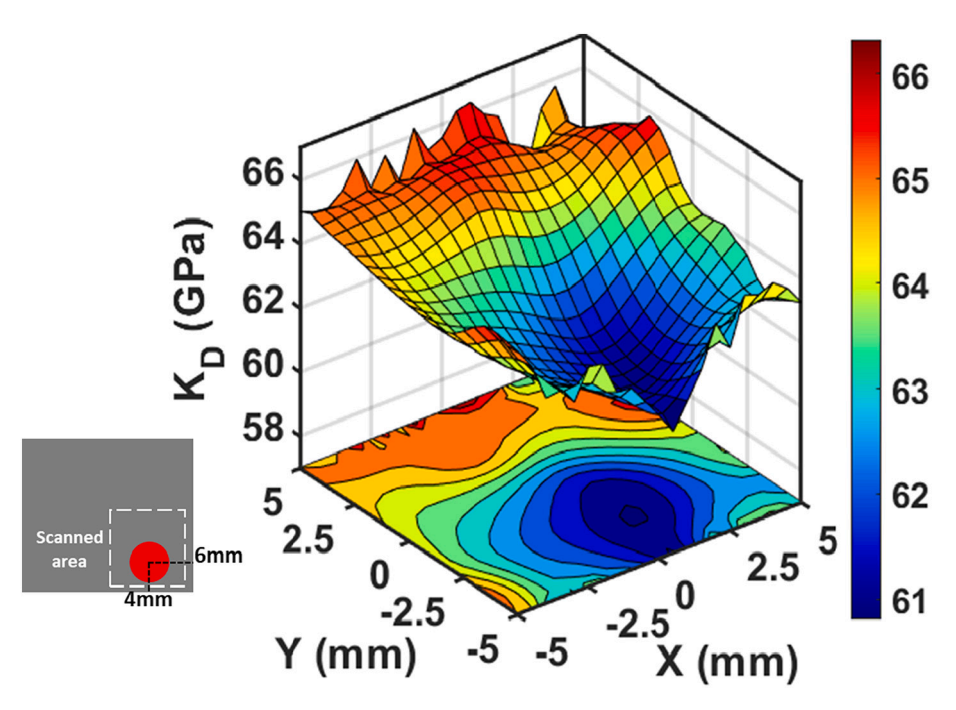


Fig. 6. Ultrasound dynamic bulk modulus elastography imaging of the sample showed in Fig. 4 after the laser induced melting. The color scale indicated the dynamic bulk modulus in the unit of GPa. The left subfigure illustrated the location of the melting pool occurred and the ultrasound scanned area. The offset of the laser induced melting pool was designed to demonstrate the capability of the elastography technique on an unequal heat dissipation result asymmetric heat affected soften region.

formation and continuous growth. In the thicker sample, the behavior of the gallium surface was examined due to the slower transition processing. The growth of melting pool depth is illustrated as a gradual process. After removing the heating source, both of the samples solidified back with a slight modification of surface conditions, which were also visualized by the ultrasound monitoring. The ex-situ dynamic elasticity distribution map illustrated the heat modified dynamic elasticity in and around the melting pool. With the commonly used operating frequency of ultrasound non-destructive testing, the attenuation of waves in metals and alloys was insignificant, which allows the acoustic pulses to penetrate decimeters easily. For the higher axial or lateral resolution of melting pool monitoring and elasticity mapping, an acoustic collimator [44] or super-resolution meta-material lens [45,46] could be further applied to increase the spatial and depth resolution of the monitoring system.

In general, based on this work, the ex-situ part of the proposed methods can be directly applied to the current laser aided manufacturing products. The elasticity distribution can be determined with additional information about the overheated or lack-of-heating phenomenon that occurred during the manufacturing. However, as the initial step of the study direction, the in-situ monitoring method is still requested long-term development to be practical for industrial cases such as laser welding and laser melting additive manufacturing. Currently, there were still many critical limitations, including thermal management, laser translation speed, and complex geometry, to directly apply the proposed in-situ method to metal AM and laser welding processing. The potential study directions in the future can be characterizing the performance of the efficiency thermal isolation, hightemperature stable ultrasound transducer, smart motion transducer arrays, and ultrasound resonance mode analysis in AM processes to overcome the limitations.

#### 4. Conclusion

In this study, we proposed a new in-situ monitoring method for determining the behavior of the laser-induced melting pool, and an exsitu method mapped out the laser-heated softened region in terms of dynamic elasticity, in the low melting point gallium system. On the insitu monitoring side, the work showed the feasibility of ultrasonic detection of the initialization, growth, and solidification behaviors of a melting pool. The parameters of the melting pool can be also estimated including the location, depth, and surface deformation which was also barely studied in the existing literature. The method performance was tested by both numerical and experimental approaches. On the ex-situ inspection side, we used recently developed dynamic bulk modulus elastography to find the dynamic elasticity drop in the laser soften region. The method has the potential to be applied in future laser-aided manufacturing applications to inspect overheated or lack-of-heating regions in the products.

#### Declaration of competing interest

The authors declare that they have no known competing financial interests or personal relationships that could have appeared to influence the work reported in this paper.

#### Acknowledgment

This work is supported by an Emerging Frontiers in Research and Innovation (EFRI) grant from the National Science Foundation (NSF) [Grant No. 1741677]; and the Center for Agile & Adaptive and Additive Manufacturing (CAAAM) funded through the State of Texas Appropriation [Grant No. 190405-105-805008-220].

#### References

- Fotovvati B, Wayne SF, Lewis G, Asadi E. A review on melt-pool characteristics in laser welding of metals. Adv Mater Sci Eng 2018;2018.
- [2] Wei HL, Knapp GL, Mukherjee T, DebRoy T. Three-dimensional grain growth during multi-layer printing of a nickel-based alloy Inconel 718. Addit Manuf 2019; 25:448-59
- [3] Moussaoui K, Rubio W, Mousseigne M, Sultan T, Rezai F. Effects of selective laser melting additive manufacturing parameters of Inconel 718 on porosity, microstructure and mechanical properties. Mater Sci Eng A 2018;735:182–90.
- [4] Rosenthal I, Stern A, Frage N. Microstructure and mechanical properties of AlSi10Mg parts produced by the laser beam additive manufacturing (AM) technology. Metallogr. Microst. Anal. 2014;3:448–53.
- [5] Farshidianfar MH, Khajepour A, Gerlich AP. Effect of real-time cooling rate on microstructure in laser additive manufacturing. J Mater Process Technol 2016;231: 468–78.
- [6] Jin Y, Wang T, Krokhin A, Choi T-Y, Mishra RS, Neogi A. Ultrasonic Elastography for nondestructive evaluation of dissimilar material joints. J Mater Process Technol 2021. https://doi.org/10.1016/j.jmatprotec.2021.117301.
- [7] Gu T, Chen B, Tan C, Feng J. Microstructure evolution and mechanical properties of laser additive manufacturing of high strength Al-Cu-Mg alloy. Opt Laser Technol 2019:112:140–50.
- [8] Chen X, Li J, Cheng X, Wang H, Huang Z. Effect of heat treatment on microstructure, mechanical and corrosion properties of austenitic stainless steel 316L using arc additive manufacturing. Mater Sci Eng A 2018;715:307–14.
- [9] Idowu OA, Ojo OA, Chaturvedi MC. Effect of heat input on heat affected zone cracking in laser welded ATI Allvac 718Plus superalloy. Mater Sci Eng A 2007;454: 389–97.
- [10] Liu S, Shin YC. Additive manufacturing of Ti6Al4V alloy: a review. Mater Des 2019;164:107552
- [11] Metel AS, Stebulyanin MM, Fedorov SV, Okunkova AA. Power density distribution for laser additive manufacturing (SLM): potential, fundamentals and advanced applications. Technologies 2019;7:5.
- [12] Li Y, Gu D. Parametric analysis of thermal behavior during selective laser melting additive manufacturing of aluminum alloy powder. Mater Des 2014;63:856–67.
- [13] Carter LN, Martin C, Withers PJ, Attallah MM. The influence of the laser scan strategy on grain structure and cracking behaviour in SLM powder-bed fabricated nickel superalloy. J Alloys Compd 2014;615:338–47.
- [14] Ziółkowski G, Chlebus E, Szymczyk P, Kurzac J. Application of X-ray CT method for discontinuity and porosity detection in 316L stainless steel parts produced with SLM technology. Arch. Civil Mech. Eng. 2014;14:608–14.
- [15] Ali H, Ma L, Ghadbeigi H, Mumtaz K. In-situ residual stress reduction, martensitic decomposition and mechanical properties enhancement through high temperature powder bed pre-heating of selective laser melted Ti6Al4V. Mater Sci Eng A 2017; 695:211–20.
- [16] Sdvizhenskii PA, Lednev VN, Asyutin RD, Grishin M Ya, Tretyakov RS, Pershin SM. Online laser-induced breakdown spectroscopy for metal-particle powder flow analysis during additive manufacturing. J Anal At Spectrom 2020;35:246–53.
- [17] V.N. Lednev, P.A. Sdvizhenskii, A. Ya Stavertiy, M. Ya Grishin, R.S. Tretyakov, R.D. Asyutin, S.M. Pershin, Online and in situ laser-induced breakdown spectroscopy for laser welding monitoring, Spectrochimica Acta part B, (2020) 106032.
- [18] Clijsters S, Craeghs T, Buls S, Kempen K, Kruth J-P. In situ quality control of the selective laser melting process using a high-speed, real-time melt pool monitoring system. Int J Adv Manuf Technol 2014;75:1089–101.
- [19] Marshall GJ, Young W Joseph, Thompson SM, Shamsaei N, Daniewicz SR, Shao S. Understanding the microstructure formation of Ti-6Al-4V during direct laser deposition via in-situ thermal monitoring. Jom 2016;68:778–90.
- [20] Zhao C, Fezzaa K, Cunningham RW, Wen H, Carlo F De, Chen L, et al. Real-time monitoring of laser powder bed fusion process using high-speed X-ray imaging and diffraction. Sci Rep 2017;7:1–11.
- [21] Rusak DA, Castle BC, Smith BW, Winefordner JD. Fundamentals and applications of laser-induced breakdown spectroscopy. Crit Rev Anal Chem 1997;27:257–90.
- [22] Lednev VN, Tretyakov RS, Sdvizhenskii PA, Grishin M Ya, Asyutin RD, Pershin SM. Laser induced breakdown spectroscopy for in-situ multielemental analysis during additive manufacturing process. Proc SPIE Int Soc Opt Eng 2018:110420R.
- [23] Lott P, Schleifenbaum H, Meiners W, Wissenbach K, Hinke C, Bültmann J. Design of an optical system for the in situ process monitoring of selective laser melting (SLM), Phys Procedia 2011;12:683–90.
- [24] Boone N, Zhu C, Smith C, Todd I, Willmott JR. Thermal near infrared monitoring system for electron beam melting with emissivity tracking. Addit Manuf 2018;22: 601–5.
- [25] Leung CLA, Marussi S, Atwood RC, Towrie M, Withers PJ, Lee PD. In situ X-ray imaging of defect and molten pool dynamics in laser additive manufacturing. Nat Commun 2018;9:1–9.
- [26] Fitzpatrick A, Singhvi A, Arbabian A. An airborne sonar system for underwater remote sensing and imaging. IEEE Access 2020;8:189945–59.
- [27] Shin S, Kim M-H, Choi SB. Ultrasonic distance measurement method with crosstalk rejection at high measurement rate. IEEE Trans Instrum Meas 2018;68:972–9.
- [28] Fu Y, Hu P, Turner JA, Song Y, Li X. Ultrasonic flaw detection for two-phase Ti-6Al-4V based on secondary scattering. NDT&E Int 2019;102:199–206.
- [29] Xue S-n, Le Q-c, Jia Y-h, Jiang L-p, Zhang Z-q, Bao L. Ultrasonic flaw detection of discontinuous defects in magnesium alloy materials. China Foundry 2019;16: 256–61.
- [30] Jin Y, Walker E, Krokhin A, Heo H, Choi T-Y, Neogi A. Enhanced instantaneous elastography in tissues and hard materials using bulk modulus and density

- determined without externally applied material deformation. IEEE Trans Ultrason Ferroelectr Freq Control 2019;67:624–34.
- [31] Jin Y, Walker E, Heo H, Krokhin A, Choi T-Y, Neogi A. Nondestructive ultrasonic evaluation of fused deposition modeling based additively manufactured 3D-printed structures. Smart Mater Struct 2020;29:045020.
- [32] Jin Y, Yang T, Heo H, Krokhin A, Shi SQ, Dahotre N, et al. Novel 2D dynamic elasticity maps for inspection of anisotropic properties in fused deposition modeling objects. Polymers 2020;12:1966.
- [33] Jin Y, Heo H, Walker E, Krokhin A, Choi TY, Neogi A. The effects of temperature and frequency dispersion on sound speed in bulk poly (vinyl alcohol) poly (Nisopropylacrylamide) hydrogels caused by the phase transition. Ultrasonics 2020; 104:105931.
- [34] Wang Z, Bao Z, Ge H, Ye Y, Jiang Z. Preparation and performance test of orthotropic piezoelectric composite material ultrasonic phased array transducer. Sens Lett 2019;17:196–200.
- [35] Shin J, Huang L. Spatial prediction filtering of acoustic clutter and random noise in medical ultrasound imaging. IEEE Trans Med Imaging 2016;36:396–406.
- [36] Tabatabaeipour M, Hettler J, Delrue S, Den Abeele K Van. Non-destructive ultrasonic examination of root defects in friction stir welded butt-joints. NDT&E Int 2016;80:23-35
- [37] Mirmahdi E. Numerical and experimental modeling of spot welding defects by ultrasonic testing on similar sheets and dissimilar sheets. Russ J Nondestruct Test 2009;56:620, 34
- [38] Pillarisetti LSS, Anandamurugan Subramanian. Ultrasonic inspection of weld defects using Total focusing method. In: Advances in Non-destructive Evaluation; 2021. p. 187–202.

- [39] Amiri N, Farrahi GH, Kashyzadeh K Reza, Chizari M. Applications of ultrasonic testing and machine learning methods to predict the static & fatigue behavior of spot-welded joints. J Manuf Process 2020;52:26–34.
- [40] Huggett DJ, Dewan MW, Wahab MA, Okeil A, Liao TW. Phased array ultrasonic testing for post-weld and online detection of friction stir welding defects. Res Nondestruct Eval 2017;28:187–210.
- [41] Konar R, Bohacik M, Mician M. Defect identification in butt weld joint by ultrasonic method phased array and X-ray technique. Manuf. Technol. 2016;16: 955-61.
- [42] Ayrinhac S, Gauthier M, Marchand G Le, Morand M, Bergame F, Decremps F. Thermodynamic properties of liquid gallium from picosecond acoustic velocity measurements. J Phys Condens Matter 2015;27:275103.
- [43] Lyall KR, Cochran JF. Velocity of sound and acoustic attenuation in pure gallium single crystals. Can J Phys 1971;49:1075–97.
- [44] Zubov Y, Djafari-Rouhani B, Jin Y, Sofield M, Walker E, Neogi A, et al. Long-range nonspreading propagation of sound beam through periodic layered structure. Commun Phys 2020;3:1–8.
- [45] Yang T, Jin Y, Choi T-y, Dahotre NB, Neogi A. Mechanically tunable ultrasonic metamaterial lens with a subwavelength resolution at long working distances for bioimaging. Smart Mater Struct 2020;30(1):015022–33.
- [46] Walker EL, Jin Y, Reyes D, Neogi A. Sub-wavelength lateral detection of tissueapproximating masses using an ultrasonic metamaterial lens. Nat Commun 2020; 11:1–13.